A Molecular Rotor Functionalized with a Photoresponsive Brake

Ryosuke Asato, Colin Martin, Seifallah Abid, Yohan Gisbert, Fumio Asanoma, Takuya Nakashima, Claire Kammerer, Tsuyoshi Kawai, Gwénaël Rapenne

A Molecular Rotor Functionalized with a Photoresponsive Brake

Ryosuke Asato[§†], Colin J. Martin[†], Seifallah Abid[#], Yohan Gisbert[#], Fumio Asanoma[§], Takuya Nakashima[§], Claire Kammerer[#], Tsuyoshi Kawai[§†] and Gwénaël Rapenne[§†#]*

§ Division of Materials Science, Nara Institute of Science and Technology, NAIST, 8916-5 Takayama-cho, Ikoma, Nara 630-0192, Japan

† International Collaborative Laboratory for Supraphotoactive Systems, NAIST-CEMES, CNRS UPR 8011, 29 rue Marvig, F-31055 Toulouse Cedex 4, France

CEMES, Université de Toulouse, CNRS, 29 rue Marvig, F-31055 Toulouse Cedex 4, France

Dedicated to the memory of Professor François Diederich (1952-2020)

ABSTRACT

A molecular motor which has been previously shown to rotate when fueled by electrons through a STM tip has been functionalized with a terarylene photochrome fragment on its rotating subunit. Photoisomerization has been performed under UV irradiation. VT ^{1}H-NMR and UV–Vis study demonstrate the rotational motion and its braking action after photoisomerization. The braking action can be reversed by thermal heating. Once the rigid and planar closed form is obtained, the rotation is effectively slowed at lower temperature making this new rotor a potential motor with independent response to electrons and light.

Preprint

Submitted to *Inorganic Chemistry*

INTRODUCTION

In the last decades, chemists have created many kinds of complex molecular architectures following a monumentalization[1-2] strategy. This approach consists of synthesizing molecules for use as elementary building blocks for the construction of more complex systems. Multifunctional nanomachines have emerged as a very dynamic area with their ingenious application based on mechanically interlocked molecules and over-crowded alkenes being recognized by the Nobel committee with the 2016 prize awarded to Jean-Pierre Sauvage, Sir J. Fraser Stoddart and Ben L. Feringa.[3] Other examples including, biomimetic nanomachines[4] such as molecular motors,[5] molecular muscles,[6] molecular walkers[7] and technomimetic nanomachines[8] like molecular scissors,[9] gears,[10] nanowheels,[11] wheelbarrows,[12] nanovehicles,[13] winches,[14] elevators[15] and robotic arms have been reported.[16] This machinery toolkit provides the basis for the future design of bottom-up nanoscale systems and materials to perform tasks as varied as nanoscale mechanics, information storage and molecular electronics.

In such models, it is very important for a multi-component molecular system to have many independent inputs controlling their motions. In our case, we recently achieved triggering and control over the step-by-step rotation of a molecular motor 2 nm in diameter deposited on a metallic surface.[5f] Depending on which part of the rotor subunit is approached by the electron injecting STM tip, we can control the rotation with about 80% unidirectionality achieved. Although this is not sufficient to lead to complete rotational control it has been observed that chirality also plays a very important role in obtaining unidirectionality.[17] The ruthenium complex used (Figure 1) contains two ligands which are not chiral however once deposited on the surface, the trisindazolyl borate and pentaphenylcyclopentadienide ligands are twisted out of the coordination plane[18] with the ruthenium complex becoming chiral. Aside from the response to electrons, light offers a further interesting independent input to switch on and off the rotation. To achieve this goal, we have designed a dual photo and electro-responsive target motor incorporating a photochromic fragment in the backbone of the rotor. The open form of such photochromes is very flexible and could allow for the rotation of the rotor, whereas once converted to its rigid closed form, the rotation could be hindered leading to rotational slowing and eventual blocking, the photochromic moiety thus acting as a light-induced brake.

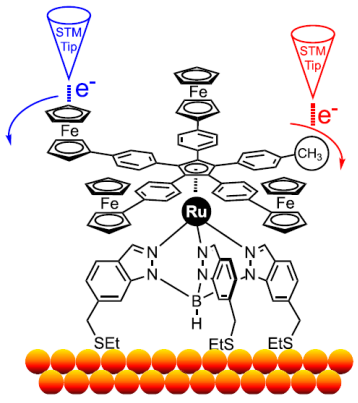

Figure 1. *Structure of the parent ruthenium-based molecular motor adsorbed on a gold surface and related electron-fueled unidirectional rotation. The tripodal ligand (stator) is anchored on the surface and the functionalized cyclopendadienyl ligand (rotor) can rotate when electrons are provided by the tip of an STM. Electron injected on one of the four ferrocenes can induce counter-clockwise rotation whereas injection in the tolyl group induce clockwise rotation.*

To devise an efficient target, the most important elements are the design of the linker and the interactions between the motor and the photochrome. In this paper, we present a computational-based molecular design to select the best combination of suitable photochromes and linkers followed by the synthesis and characterization of the selected target. The steric hindrance between the photochrome-substituted rotor and the stator is a key parameter. More precisely, to obtain an efficient brake function, we need to tune the intramolecular interactions to select geometries allowing for blocking of the rotation once linked to the motor. This is proposed to be done by having the rigid closed form of the selected photochrome lie between two of the three legs of the stator part, hindering rotation, while the flexible open form of the photochrome will not interact with the stator, leaving the system free to rotate. Our concept is illustrated in Figure 2.

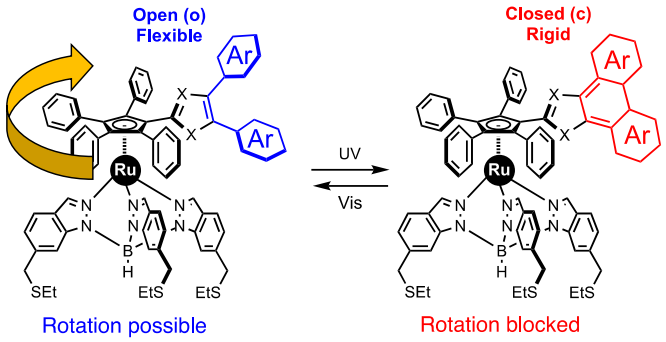

Figure 2. *Schematic representation of the difference between the open- and closed-forms of the targeted photochrome-substituted molecular motor. Upon application of UV light, the closed-form of the photochrome is obtained preventing the rotation of the rotor part of the motor.*

This brake function would be complementary to the rotation of our motor which is induced by electrons and controlled at will in clockwise or anti-clockwise directions. Our motors would then integrate two independent input signals: electrons as the source of energy to rotate and light which could allow or slow the process at will.

RESULTS AND DISCUSSION

Design of the photochromic molecular motor

For the successful integration of the proposed photochromic brake into the existing motor framework we identified a number of contributing factors initially needed to be optimized to allow for its operation, in particular the nature of the photochromic moiety, and the linker between the photochrome and the motor. The latter needs to be short with a controlled directionality to allow the photochrome (i.e. the brake when closed form) to block the rotation by interaction with the stator (the tripodal ligand). To select the most suitable target, Gaussian DFT calculations have been performed using the hybrid dispersive ωB97xD functional[19] to obtain the energy minimized geometries of the open and the closed form of the photochrome-functionalized molecular motor. The optimal target being the one with the largest steric blocking interactions upon photoisomerism between the flexible open form and the rigid closed form.

A number of photochromic moieties with the potential to act as a brake were identified, based upon previous reports of diarylethene and terarylene photochromic properties.[20] Each photochrome-substituted molecular motor was modelized and geometry was optimized in their open and closed photochromic isomers to estimate the changes brought about by ring closure and the resulting effect on rotational motion through steric interactions with the stator part of the molecular motor. These interactions were evaluated qualitatively thanks to the optimized geometries of both isomers of each molecule calculated in the gas phase but giving insightful clues on the ability to rotate and brake of each molecular motor. Videos displaying a 360° rotation of the molecules allowing for a better illustration of the steric hindrances are provided as Supplementary Material to this paper.

The design of the photochromic part was initially considered in terms of the switching efficiency and the geometries obtained before and after. As such, it was decided to use an initial photochromic core framework which can be conjugated to the cyclopentadiene part of the motor (Figure 3, left) rather than one of the peripheral side rings that undergo ring closure (Figure 3, right). To achieve this, a terarylene core was chosen rather than a diarylethene due to the extra rigidity it offers through the central core aromatic ring compared to the more flexible ethynyl core offered by diarylethene. The photochromic terarylene consists of three heteroaromatic rings to form a photoreactive hexatriene framework in its molecular structure, which undergoes reversible photoinduced cyclization to a closed-ring isomer. As previous studies on molecular motors have shown that the aromatic substituents on the cyclopentadiene ring rotate out of the plane,[21] substitution on the core of the terarylene also offers a conformation in the closed form expected to lead to larger steric interactions between the photochromic and stator parts of the molecule which is important to induce blocking of the rotation by the photochromic part in the closed form.

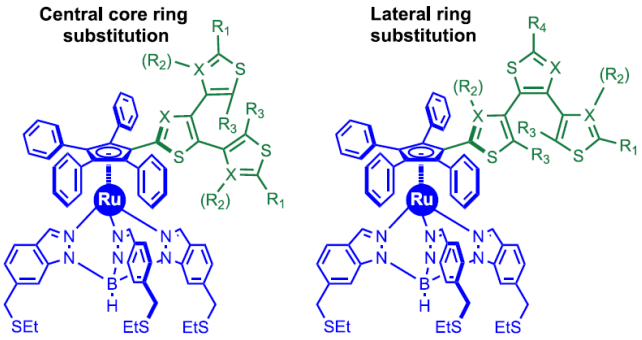

Figure 3. *Motor (in blue) with two possible photochromic terarylene substitution patterns (in green). X = C (thiophene) or N (thiazole, with no R_2)*

We decided to use a combination of thiazole and thiophene rings as the core and peripheral cycles within the photochromic moiety. The presence of both of these substituents is advantageous in terms of conformational preference and is known to maximize the donor-acceptor properties leading to efficient ring opening and closing and higher photochromic quantum yields.[22] For the initial braking systems it was decided to use methyl substituents (Figure 3, R_3) at the positions of photochromic bond formation as this is known to lead to stable, reversible photochromic switching.[23] Based on these considerations five target photochromic frameworks **T1** – **T5** (Figure 4) were selected for initial calculations and to screen the effect of substituents present (Figure 3, R_1 and R_2) upon their incorporation into the motor frameworks **MM-T1** – **MM-T5**.

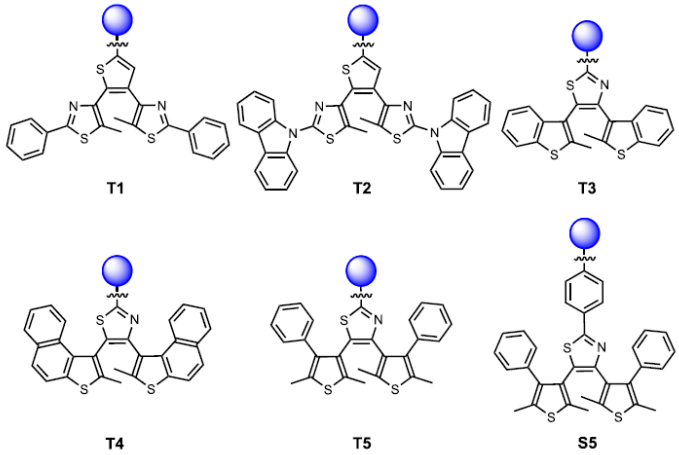

Figure 4. *Preselected photochromic moieties* ***T1-T5*** *and* ***S5*** *for incorporation into the motor backbone. The blue spheres represent the motor fragment.*

Each was modelled computationally using the Gaussian 09 DFT program operating using the ωB97xD functional and the 6-31G(d,p) basis set[19] for all atoms except ruthenium for which LANL2DZ[24] was used.

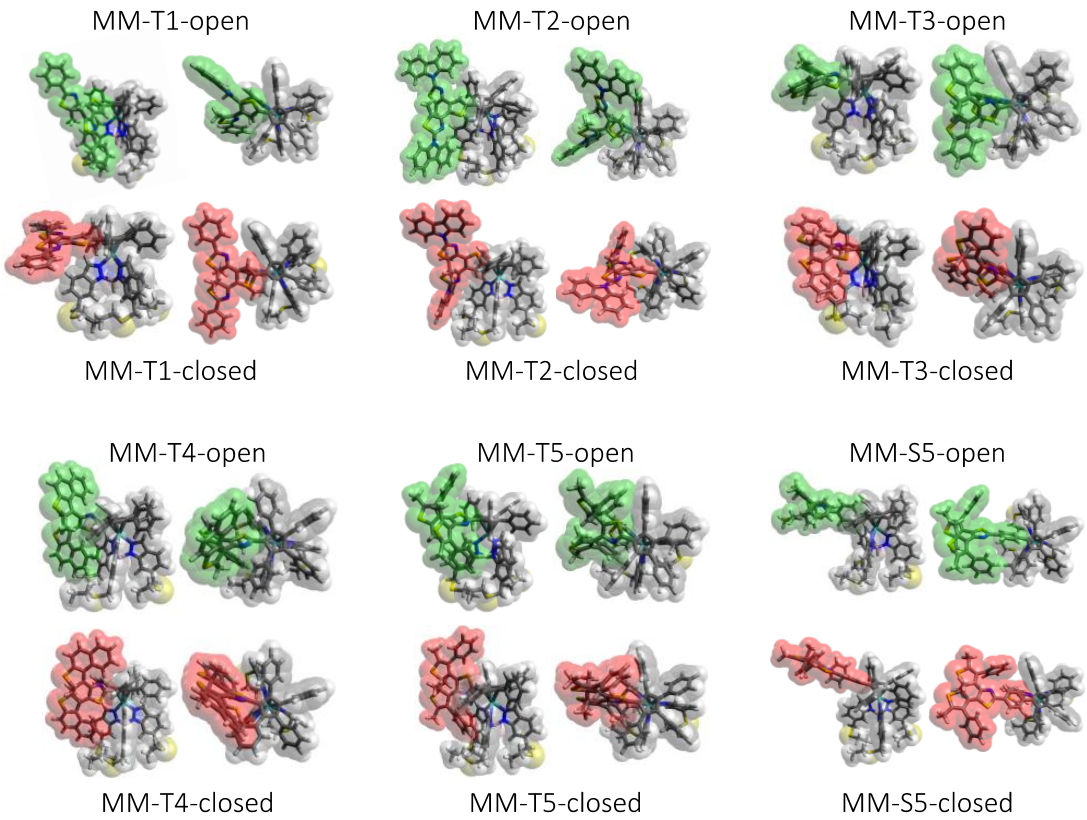

Figure 5. *Optimized geometries as side and top views of the open and closed forms of the molecular motors* ***MM-T1*** *to* ***MM-T5*** *and* ***MM-S5*** *functionalized with photochromic moieties* ***T1-T5*** *and* ***S5****. The π-systems involved in the photochromic isomerization are indicated in green for the open and red for the closed forms.*

For the systems containing a thiophene central ring and thiazole peripheral rings (**MM-T1** and **MM-T2**) the absence of a sterically bulky substituent at the thiazole 3-position meant no steric interactions between the photochrome and the stator in either their open or closed isomers was observed (Figure 5). In the case of **MM-T1** (see SI) the absence of any interaction with the stator, even in the closed form, lead to the central thiophene ring of the photochrome lying coplanar to the cyclopentadiene ring of the rotor, resulting in the photochrome pointing away from the stator even in the closed isomer. For the three systems containing a thiazole central ring and thiophene based peripheral rings (**MM-T3** to **MM-T5**) the increased steric hindrance resulting from substitution at the thiophene 4-position led to the presence of the desired braking interactions in the closed form. As such, it was decided to use a thiazole as the central core ring connected to the motor and thiophenes substituted at the 4-position as the peripheral photochrome rings.

In the DFT calculations of these systems (**MM-T3** to **MM-T5**), the open form appears highly flexible and shows no apparent interactions between the photochrome and the stator. However, upon switching to the closed form the increased rigidity of the photochrome, in conjunction with the angle between the cyclopentadiene ring and the connected benzothiophene ring of the photochrome (49° for **MM-T3**), leads to the rigid closed form taking up a position pointing between two of the three legs of the stator. To help to visualize the steric hindrance, a 3D animation movie is available (supporting information) in the case of **MM-T3** (open and closed forms). Such geometries are predicted to result in cessation of the rotation of the molecule as the 'brake' is applied upon switching from the open to closed photochromic forms.

To examine the effect of varying the distance between the photochrome and the cyclopentadienyl core and to potentially simplify the synthetic method, a phenyl spacer was inserted between the motor and the photochromic system to give **MM-S5**, the extended photochrome derivative of **MM-T5**, and the DFT calculation was repeated. However, in the presence of the spacer both the open and closed forms of **MM-S5** show no steric interactions. This led us to conclude that the terarylene photochrome is required to be substituted directly on the cyclopentadiene ring of the rotor to induce rotational blocking further developing the requirements in our molecular design.

Of the remaining designs of molecular motors functionalized with photochromes **T3**, **T4** and **T5**, **MM-T3** (Figure 5) appears to offer the best initial target as a molecular brake for several reasons: 1) It has the lowest amount of interactions between the open photochromic form and the stator, meaning the system will find it easier to rotate prior to application of the light brake. 2) It also contains the highest levels of hydrogen bonding (CH/S and CH/N) between the constituent rings of the photochromic moiety; such interactions are known to lead to higher ring closure quantum yields which will make the braking mechanism more photon efficient. 3) It shows a strong blocking interaction between the closed form isomer and the stator similar to that of other targets with the closed form lying between two legs of the stator. 4) Its relative synthetic simplicity as an initial target molecule compared to **MM-T4** and **MM-T5**. As such we decided to incorporate **T3** as the photochromic part of our initial molecular brake motor referred as **MM-T3** (Figure 6).

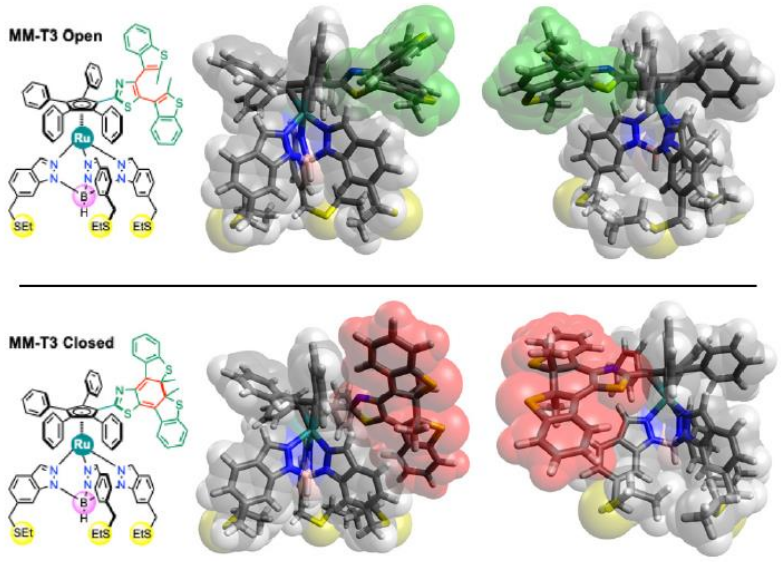

Figure 6. *Open (top) and closed (bottom) forms of* ***MM-T3****, showing the changes in interaction between the stator and the photochromic moiety. The π-system involved in the photochromic isomerization is indicated in green for the open and red for the closed forms. A 3D animation movie is available as a supporting information to help to ease the visualization of the interactions.*

Synthesis of the photochrome-substituted motor

The synthesis of the photochrome-functionalized motor **MM-T3** was achieved in five steps with a global yield of 4.5% (Scheme 1 and 2). The synthesis of the required terarylene 4,5-bis(2-methyl-1-benzothiophen-3-yl)-1,3-thiazole (**T3**) was first tackled. To start with, 4,5-dibromo-1,3-thiazole **1**[25] was coupled to 4,4,5,5-tetramethyl-2-(2-methyl-1-benzothiophen-3-yl)-1,3,2-dioxaborolane (**2**[22]) through Suzuki-Miyaura coupling to give terarylene **T3** in a 74% yield after purification by column chromatography. **T3** was then lithiated at the 2-position of the thiazole ring using *n*-butyllithium and reacted with 2,3,4,5-tetraphenylcyclopentadienone to give the tetraphenylcyclopentadienol **4** in 63% yield. Unlike in the precursor **T3** only one rotational conformer of **4** is seen in the NMR spectrum, resulting from hydrogen bonding between the alcoholic proton and the thiazole nitrogen favoring one conformation in solution. **4** was then converted to its chloride analog **5** by reaction with thionyl chloride in benzene in a yield of 90%. This chloride analogue consists of three regioisomers present in a non-stoichiometric ratio, leading to highly complex NMR data for **5**.[26] The presence of this chlorine allowed us to coordinate the cyclopentadiene ring to the ruthenium atom, with oxidative addition of the triruthenium dodecacarbonyl cluster at the carbon-chlorine bond of all regioisomers of **5** leading to the same metal complex. The cyclopentadienyl ruthenium(II) complex **6** was obtained as a bright yellow solid in 56% yield, with two conformational isomers observed in the ^{1}H NMR with a 2:1 ratio observed in the methyl peaks.

Finally, coordination of the tris[(ethylsulfanyl)methyl]indazolylborate ligand was performed by reaction of the ruthenium cyclopentadienyl complex **6** with two equivalents of the thallium salt of the hydrotris(indazolyl)borate derivative[27] by microwave heating in acetonitrile at 100 °C (Scheme 2). Due to the evolution of carbon monoxide during the reaction, the pressure was released every 10 min and the conversion followed by TLC of the crude mixture. The target photochromic motor **MM-T3** was obtained in 20% after 1 hour. Each compound was characterized using NMR and mass spectral data,

however the presence of multiple conformational and rotational isomers made complete assignment of the NMR spectroscopic data difficult due to significant broadening of signals.

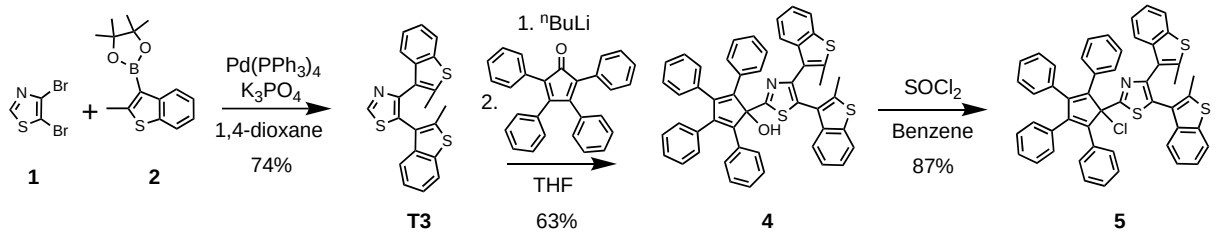

Scheme 1. *Synthesis of the cyclopentadiene rotor functionalized with a terarylene fragment (**5**).*

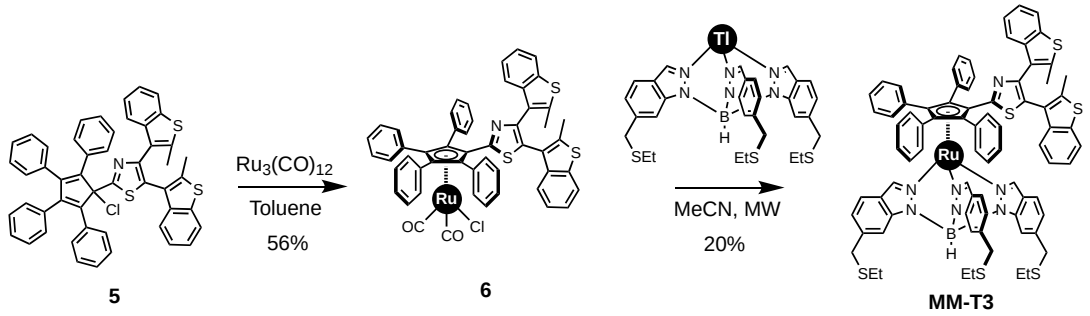

Scheme 2. *Synthesis of the photochromic motor **MM-T3** incorporating a terarylene brake.*

Photoswitching of the precursor (4)

To examine the effect of illumination upon the motor structure, a ^{1}H NMR study was carried out. Initially the photochromic switching of the precursors was examined; due to the relative stabilities of the molecules it was decided to look at the alcohol **4** as a representative example. To allow for comparison with **MM-T3**, this was done in CD_2Cl_2. Here, sharp signals are observed at 7.68, 7.64 and 6.83 ppm for three of the four photochrome benzothiophene protons, along with a large broadened region between 7.45 and 6.90 ppm masking the fourth benzothiophene signal (Figure 7 top). This broadening of the aromatic region is consistent with what is seen for the photochromic precursor **T3** along with observations of similar non-photochromic cyclopentadienyl systems and results from the high rotational barriers for benzothiazole substituents in the terarylene core on the timescale of NMR. The methyl substituents present at the sites of photoinduced bond formation further hinder rotation and as such there are a number of similar but not identical environments for these protons, further broadening the signals.[8,18,27] Due to this broadness a precise integration is not possible, however approximate values show an integration of twenty-eight protons relative to the alcohol OH singlet at 4.71 ppm. Along with this, broad signals for the methyl substituents on the photochrome, integrating for six protons, are observed between 1.98 and 1.75 ppm.

As at the illumination wavelengths required both open to closed and closed to open switching can occur, isolation of a solution containing 100% of the closed form was not possible. Instead the photostationary state (PSS) was prepared to allow observation of a solution containing a majority of closed form isomers. Based on previous reports on the efficiencies of ring closing and opening of the photochromic framework a PSS containing greater than 80% closed form is expected.[28] The sample was dissolved in

hexane and illuminated for 30 minutes at 254 nm, solvent removed, and the solution redissolved in deuterated dichloromethane to examine the spectrum of the PSS (Figure 7, bottom).

It can be seen that some changes occur in the aromatic peaks, however more significantly there are shifts seen in the methyl peaks between 1.98 and 1.75 ppm, indicating that photochromic ring closure has taken place with the appearance of structural isomers in both the open and closed forms. This is consistent with the absorption spectra of **4** where new bands showing the formation of a photostationary state (Figure 7, inset) including some closed form are observed, which returns to the absorption profile of the open form upon application of light above 400 nm.

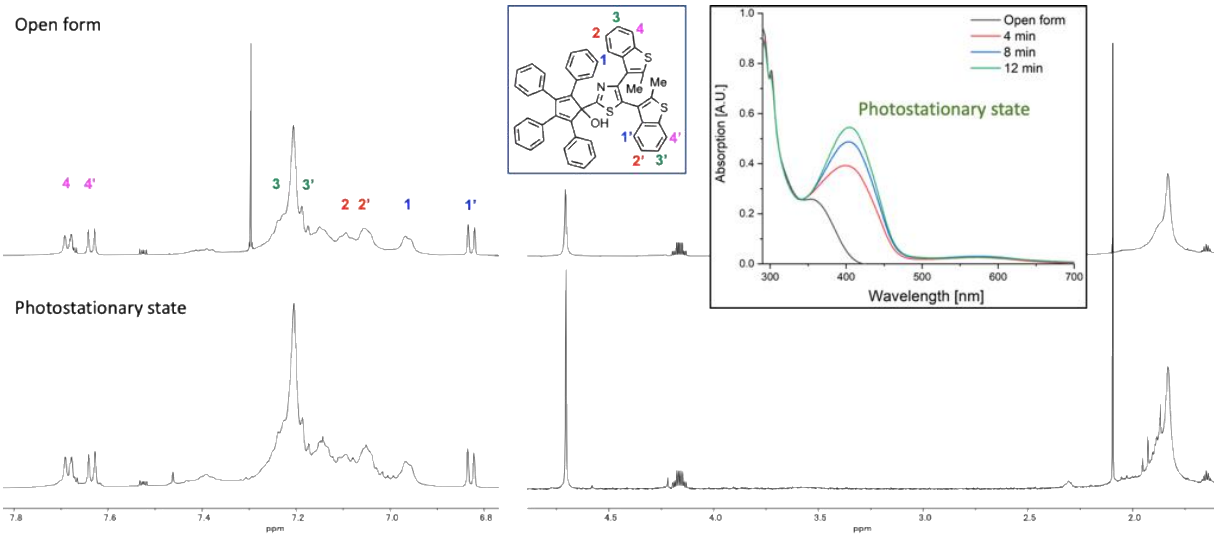

Figure 7. *Photoswitching of the precursor (**4**) by illumination at 254 nm followed by UV-Vis. (CH_2Cl_2) spectroscopy (Inset) and by ^{1}H-NMR (600 MHz) in CD_2Cl_2. At the top is shown the open form and at the bottom the photostationary state. Assignments were made with the assistance of COSY, NOESY, HMQC and HMBC of the sample run at 500 MHz in CD_2Cl_2.*

Photoswitching of the photochromic ruthenium complex (MM-T3)

Next the ^{1}H NMR of **MM-T3** was run in deuterated dichloromethane. Broad aromatic peaks are again seen between 7.80 and 6.80 ppm, indicating the presence of the cyclopentadiene rotor. Four further aromatic peaks are seen, each integrating for three protons (with two overlapping), for the protons located on the tripodal stator indazolyl fragments. These can be assigned based on previous reports with H^1 and H^6 (Figure 8, top) appearing downfield at 8.32 and 7.83 ppm and H^3 and H^4 overlapping for a total integration of six protons between 6.96-6.92 ppm. The signals for the aliphatic stator chains can also be observed with H^7 appearing as a singlet at 3.87 ppm, a quartet for H^8 at 2.44 ppm and H^9 appearing as a triplet at 1.26 ppm. Also very broad signals indicating the presence of multiple conformational and rotational isomers are seen between 2.0 and 1.7 ppm for the photochrome methyl substituents. Despite the apparent broadness the expected signals for the cyclopentadienyl rotor, the photochromic brake and the indazolylborate stator can be seen in the ^{1}H NMR of **MM-T3**.

To resolve the broad peaks and to observe the effect of thermal cooling on the rotation, the ^{1}H NMR of **MM-T3** was run at 10 K decrements between 293 K and 233 K (Figure 8, see SI for full thermal data). At 273 K the two overlapping stator peaks between 6.96 and 6.92 ppm begin to separate. Upon further cooling to 253 K all four of the aromatic stator peaks split into two resulting from the rotation slowing

as the solution cools. Upon rotational 'braking', a 2:1 splitting of these peaks is expected, with two of the stator legs remaining equivalent and the other becoming independent. Indeed, it is stator proton H^1 that points towards the rotor that shows the largest thermal splitting. Upon further cooling to 233 K a further increase in resolution of the aromatic signals is observed, however this is not enough to allow for their further characterization. Such splitting of the stator protons offers a clear measure of the changes in the rotational environment of **MM-T3**.

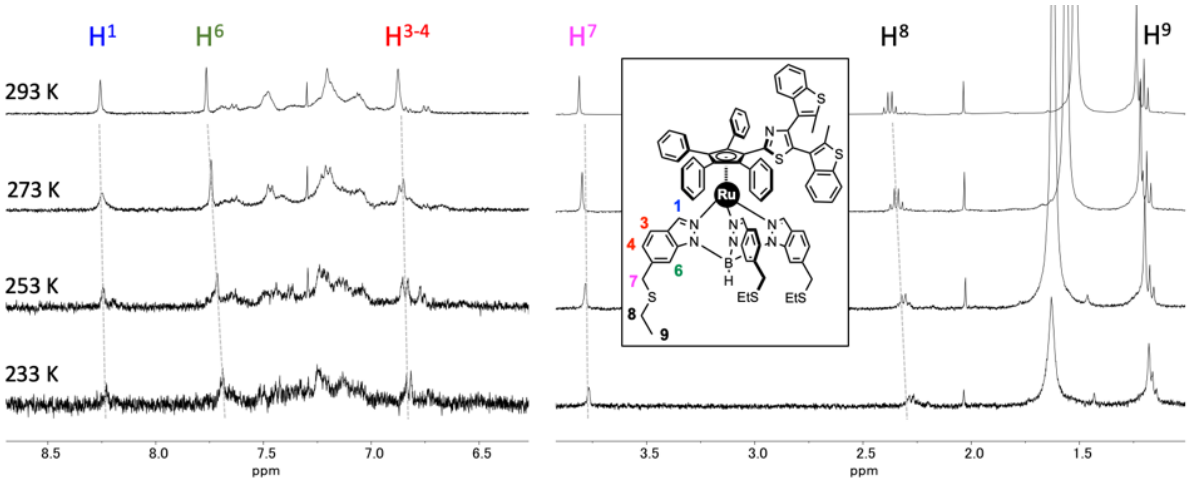

Figure 8. *^{1}H-NMR of **MM-T3** (Open form) at 293, 273, 253 and 233 K in CD_2Cl_2 (400 MHz).*

To examine the effect of illumination on **MM-T3**, it was next exposed to UV light (254 nm, 6W, 265 mW/cm^2) for 15 minutes and the ^{1}H NMR before and after compared (Figure 9, top and middle). Illumination results in a rapid broadening of the aromatic stator signals along with the formation of some new peaks in the broadened cyclopentadienyl region. This rapid broadening is indicative of a significant change in the molecules rotational ability upon ring closure, resulting from the now closed bulky photochrome. Upon ring closure the rotation of the molecule becomes hindered by the closed form photochrome, with the rotation becoming more difficult due to the increasing rotational energy barriers. It is important to note however that unlike in the case of temperature decrease this does not lead to a splitting of the stator peaks. Thus, it can be assumed that while the rotation of the motor may be greatly hindered, it is not completely stopped at room temperature. However, the observation of this broadening even under room temperature NMR conditions, indicates the possibility of obtaining complete light induced rotational 'braking' under different conditions, including those employed for STM analysis. It should be mentioned that no decomposition nor decoordination of the cyclopentadienyl or the tripodal ligand was observed, each fragments having characteristic peaks which did not appeared in any of the NMR spectra of the illuminated **MM-T3** '(Figure S13).

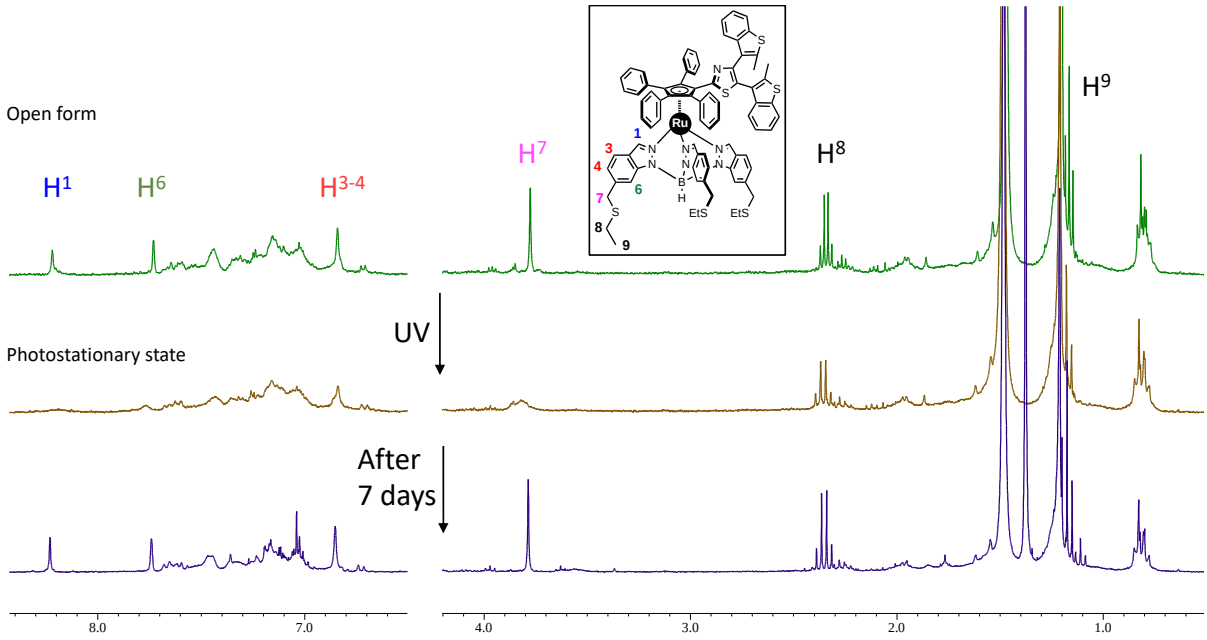

Figure 9. *^{1}H-NMR of **MM-T3** before (top) and after (middle) illumination along with after seven days (bottom) in CD_2Cl_2 (500 MHz).*

Next the sample was illuminated using orange (above 550 nm) light in an attempt to return the closed photochrome to its open form, however NMR showed that the sample remained in the closed form even after illumination for 15 min. This can be attributed to a combination of the competition in absorption between the photochrome and the ruthenium center at these frequencies and energy quenching of the ligand-centered excited state by the ruthenium center. Instead the system was left in the dark for seven days to allow the ring opening to occur thermally. NMR analysis after this time showed the successful reversion to the open form, indicating full thermodynamic release of the "brake" over time (Figure 9, bottom).

To further examine the change in **MM-T3** with light, its absorption profile before and after illumination was observed and compared with calculated DFT values. In dichloromethane (Figure 10, left, black line) the open form of **MM-T3** shows absorption bands between 400 and 600 nm similar to those reported for similar non-photochromic motors.[27,29] TD-DFT calculations show these absorptions as ruthenium centered coming mainly from the metal dominated HOMO-1 orbital level. Upon formation of the photostationary state only small changes are seen, indicating absorption by the ruthenium center is not significantly affected by photochromic ring closure. To monitor these changes, the difference in absorption between the PSS and the open form was calculated (Figure 10 left, inset). This shows two broad areas of increased absorption about 344 and 534 nm. This was compared to the changes predicted between the closed and open forms by DFT (Figure 10, right) which showed increases around 334 and 471 nm. Both experimental and DFT absorptions in the region expected to induce ring opening of the photochromic unit (400-600 nm) appear overlapped with the ruthenium centered absorptions. This further explains the lack of photoreversion to the open form upon illumination above 550 nm despite **MM-T3**'s ability to ring open thermodynamically over time.

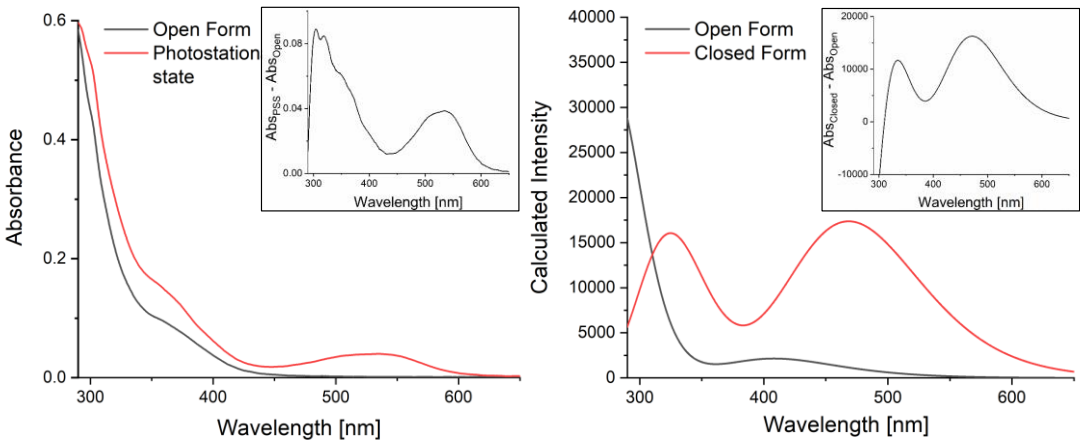

Figure 10. *Comparison of the measured (left) and DFT calculated (right) absorptions of* ***MM-T3*** *in* CD_2Cl_2*. Insets show the difference between the closed and photostationary states (red) from the open form (black).*

CONCLUSION

In this work, a previously reported molecular motor has been functionalized with a terarylene photochromic fragment and fully characterized. VT-NMR showed that the rotation of the functionalized cyclopentadienyl ligand becomes blocked when the closed form is generated by the application of light and its rotation is drastically hindered. Work is now underway to investigate by STM the complementary functionality of the light to block electron-induced rotation of our motor on surfaces.

EXPERIMENTAL SECTION

Materials and instrumentation

All commercially available chemicals were of reagent grade and were used without further purification. Column chromatography was carried out on 230–400 mesh silica gel (Aldrich) unless otherwise stated. Compound **1**[25], **2**[24] and the thallium salt of hydrotris[(ethylsulfanyl)methyl]indazolylborate[27] were synthesized as previously reported.

Microwave reactions were carried out by using a CEM Discover LabMate microwave reactor. TLC was performed on precoated aluminum-backed silica gel 60 UV254 plates (Macherey-Nagel) with visualization by UV irradiation (λ =254, 366 nm). ^{1}H-NMR (500 MHz) and ^{13}C-NMR (125 MHz) spectra were recorded on Bruker Avance III HD 500 MHz, ^{1}H-NMR (600 MHz) spectra were recorded on JEOL JNM-ECA600 and VT NMR were recorded on JEOL JNM-ECX400P. Residual solvent signals were used as internal references for ^{1}H and ^{13}C-NMR spectra which were referenced according to the solvent. IR spectra were recorded with a Nicolet 6700 FTIR-ATR spectrometer. Only selected characteristic peaks were recorded. Recycling preparative GPC were performed on LC-9110NEXT (Japan Analytical Industry). Reverse Phase HPLC were performed on LaChrom Elite (Hitachi). High-resolution mass spectra were obtained with a Waters GCT Premier spectrometer for desorption chemical ionization (DCI/CH4), with a Waters Xevo G2 QTof spectrometer for electrospray ionization (ESI) with a Bruker Autoflex II and with a JEOL JMS-Q1000TD and JMS-700 Mstation. UV-Vis absorption spectra were obtained on JASCO V-550, JASCO V-660 and JASCO V-760, Shimadzu UV-26000 spectrometer. Light source of UV (254 nm and 365 nm) was AS ONE SLUV-4.

All calculations were performed with the Gaussian09 package[30] using the hybrid dispersive ωB97xD functional and the 6-31G(d,p) basis set which can represent all atoms up to argon. The LANL2DZ functional operating with a pseudopotential, was used for the ruthenium. Geometry optimization was performed in vacuum and followed by a frequency calculation showed no negative frequencies confirming that resulting structures were in a minimum of the potential map. TD-DFT calculations were performed at the same level of theory for the open and closed form of **MM-T3** using the previously optimized geometry as a starting point taking the dichloromethane solvent into account using a PCM model in order to obtain comparable UV-VIS spectra.

Synthesis and characterization

4,5-bis(2-methylbenzo[b]thiophen-3-yl)thiazole (T3)

4,5-Dibromo-1,3-thiazole (**1**) (1 eq., 1.00 g), 4.12 mmol) and 4,4,5,5-tetramethyl-2-(2-methyl-1-benzothiophen-3-yl)-1,3,2-dioxaborolane (**2**) (2.3 eq., 2.60 g, 9.47 mmol) were dissolved in 1,4-dioxane (15 mL) and aqueous tripotassium phosphate (2 M, 15 mL) was added dropwise. The solution was bubbled with N_2 for 15 min. Then, tetrakis(triphenylphosphine)palladium (5 mol%, 0.230 g, 0.206 mmol) was added and the solution stirred under reflux for 36 hours. After cooling down to room temperature, the solution was extracted by ethyl acetate and washed with water and saturated aqueous solution of sodium chloride. The organic layer was dried with anhydrous sodium sulfate, filtered, and concentrated. Silica gel column chromatography (9:1 hexane:ethyl acetate) gave a white solid (1.1 g, 74%). ^{1}H-NMR (500 MHz, CD_2Cl_2, 25ºC) δ (ppm) 2.02 (m, 6H), 7.20-7.29 (m, 4H), 7.56 (s 2H), 7.72-7.74 (m, 2H), 9.14 (s, 1H), NMR consistent with previous report.[28]

1-(4,5-bis(2-methylbenzo[b]thiophen-3-yl)thiazol-2-yl)-2,3,4,5-tetraphenyl-cyclopenta-2,4-dien-1-ol (4)

4,5-Bis(2-methyl-1-benzothiophen-3-yl)-1,3-thiazole (**T3**) (1 eq., 0.70 g, 1.85 mmol) was dissolved in 50 mL of degassed anhydrous tetrahydrofuran and cooled down to -78 ℃. *n*-Butyllithium (1.6 eq., 2.3 M, 1.29 mL, 2.97 mmol) was added dropwise while keeping at this temperature. The solution turned brown-red, and was stirred for 2 hours at this temperature. Then, 2,3,4,5-tetraphenylcyclopentadienone (2.36 eq., 1.68 g, 4.37 mmol) was dissolved in 50 mL degassed anhydrous tetrahydrofuran and cannulated dropwise into the solution. The resulting solution was stirred for 1 hour at -78℃ and allowed to warm to room temperature and stirred for 1 hour. Finally, 5 mL of saturated aqueous ammonium chloride was added slowly. The solution was extracted by ethyl acetate and washed with water and a saturated aqueous solution of sodium chloride. The organic layer was dried with anhydrous sodium sulfate, filtered, and concentrated. Silica gel column chromatography (2:1 dichloromethane:hexane) gave a white solid (0.89 g, 63%). (500 MHz, CD_2Cl_2, 25ºC) δ (ppm) 1.86-1.90 (m, 6H), 4.75 (s, 1H), 6.86 (d, ^3J = 7.8 Hz, 1H), 7.00-7.46 (m, 22 H), 7.66 (d, ^3J=8.4 Hz, 1H), 7.71 (d, ^3J=7.8 Hz, 1H). ^{13}C NMR (125 MHz, CD_2Cl_2, 25ºC) 14.8, 14.9, 90.1(>C*OH*), 121.9, 122.1, 122.3, 122.9, 123.1, 124.1, 124.5, 124.6, 124.9, 126.8, 127.7, 127.9, 128.1 ,128.4, 129.4, 129.9, 130.0, 134.0, 134.2, 134.9, 135.1, 138.1, 138.2, 139.6, 139.7, 140.2, 141.1, 146.5, 171.8 (-C*SN*). HRMS (DCI/CH_4) (*m/z*): $[M]^+$ calcd. for $C_{50}H_{35}NOS_3$ 761.1881; found 761.1882.

2-(1-chloro-2,3,4,5-tetraphenylcyclopenta-2,4-dien-1-yl)-4,5-bis(2-methyl benzo[b]thiophen-3-yl)thiazole (5)

1-[4,5-Bis(2-methyl-1-benzothiophen-3-yl)-1,3-thiazol-2-yl]-2,3,4,5-tetraphenylcyclopenta-2,4-dien-1-ol (**4**) (1 eq., 50 mg, 0.066 mmol) was dissolved in 2 mL of benzene. Thionyl chloride (6 eq., 69 mg, 0.042 mL, 0.58 mmol) was slowly added, and the solution heated to reflux. After heating for 30 min, the solution was allowed to cool down to room temperature. An orange solution was purified by silica gel column chromatography (1:1 dichloromethane:hexane) to give compound **5** as yellowish orange powder. (45 mg, 87%). ^{1}H-NMR (500MHz, CD_2Cl_2, 25ºC) shows broad signals in the aromatic region due to three regioisomers present in a non-stoichiometric ratio, see SI (Fig. S4) for the full spectrum . δ (ppm) 1.51-2.03 (6H, CH_3 peaks), 6.62-7.45 (24 H, aromatic signals), 7.57-7.74 (4H, aromatic signals). ^{13}C-NMR (125 MHz, CD_2Cl_2, 25ºC) δ (ppm) shows complex signals in the aromatic region due to three regioisomers present in a non-stoichiometric ratio, see SI (Fig. S5) for the full spectrum. 14.5 (C*H*$_3$), 14.6 (C*H*$_3$), 15.2 (C*H*$_3$), 58.4 (>C*Cl*), 121.3, 121.4, 121.8, 121.9, 123.5, 123.6, 124.1, 124.6, 126.5, 127.5, 127.6, 127.7, 127.8, 128.0, 128.3, 128.5, 128.8, 129.0, 129.2, 129.5, 130.0, 130.3, 133.4, 134.2, 134.6, 137.8, 137.9, 140.4, 147.9, 159.2. HRMS (ESI) (*m/z*): $[M+H]^+$ calcd. for $C_{50}H_{35}ClNS_3$ 780.162; found 780.167. HRMS (ESI) (*m/z*): $[M+H]^+$ calcd. for $C_{50}H_{35}ClNS_3$ 780.162; found 780.167.

Chlorodicarbonylη^5-1-(4,5-bis(2-methylbenzo[b]thiophen-3-yl)thiazol-2-yl)-2,3,4,5-tetraphenylcyclopentadienyl]ruthenium(II) (6)

2-(1-Chloro-2,3,4,5-tetraphenylcyclopenta-2,4-dien-1-yl)-4,5-bis(2-methyl-1-benzothiophen-3-yl)-1,3-thiazole (**5**) (1 eq., 44 mg, 0.0564 mmol) and triruthenium dodecacarbonyl cluster (0.6 eq., 21.6 mg, 0.0338 mmol) were introduced. Anhydrous and degassed toluene (2 mL) was then added. The mixture was heated to reflux for 2 h under argon. Then the solution was allowed to cool down to room temperature, the organic layer concentrated and purified by column chromatography (1:1 dichloromethane:hexane) to give compound **6** as bright yellow solid (30 mg, 56%). ^{1}H-NMR (500 MHz, CD_2Cl_2, 25ºC, TMS) δ(ppm) shows two conformational isomers. 1.63 (s, 2H, CH_3 isomer peak), 1.80 (s, 2H, CH_3 isomer peak), 2.06 (s, 1H, CH_3 isomer peak), 2.34 (s, 1H, CH_3 isomer peak), 6.37-7.84 (28 H, aromatic signals). ^{13}C NMR (125 MHz, CD_2Cl_2, 25ºC) shows broad signals due to the presence of two conformational isomers, see SI-Fig. S9 for the full spectrum δ (ppm) 14.6 (-C*H*$_3$), 14.8 (-C*H*$_3$), 77.6 (>C*Cl*), 113.0, 115.4, 121.6, 122.1, 124.4, 124.6, 124.9, 127.6, 127.7, 128.0, 128.2, 128.4, 131.7, 133.7, 138.1, 139.1, 142.1, 144.0, 205.0 (*CO*), 205.8(*CO*). IR (ATR, solid): cm^{-1} 2360 (*CO*), 2342 (*CO*).

η^5-1-(4,5-bis(2-methylbenzo[b]thiophen-3-yl)thiazol-2-yl)-2,3,4,5-tetraphenylcyclopentadienyl hydrotris{6-[(ethylsulfanyl)methyl]indazol-1-yl}borateruthenium(II) (MM-T3)

In a glove box, in a dried reactor specifically designed for microwave irradiation under argon were successively added a magnetic stirrer bar, chlorodicarbonyl[(1,2,3,4,5-η)-1-(4,5-bis(2-methylbenzo[b]thiophen-3-yl)thiazol)-2,3,4,5-tetraphenyl-2,4-cyclopentadien-1-yl]ruthenium(II) (**6**) (1 eq., 32 mg, 0.0341 mmol), thallium hydrotris{6-[(ethylsulfanyl)methyl]indazol-1-yl}borate (2.5 eq., 64.4 mg, 0.0815 mmol) and degassed acetonitrile (8.38 mL). The reaction mixture was heated to 100°C six times for 10 min in each heating cycle. A pressure of 5 bar was achieved and it was released between heating cycles. The completion of the reaction was monitored by TLC. The resulting mixture was diluted with dichloromethane and filtered through silica gel. The solvents were removed under reduced pressure and the residue was purified by column chromatography (2:1 dichloromethane:hexane) to afford compound **MM-T3** (9.8 mg, 20%) as a brown solid. ^{1}H-NMR (500MHz, CD_2Cl_2, 25ºC, TMS) δ (ppm)

1.26 (t, ^3J=7.4 Hz, 9H), 2.44 (q, ^3J=7.3 Hz, 6H), 3.87 (s, 6H), 6.92-6.96 (m, 6H), 6.99-7.69 (m, broad signals due to conformational and rotational isomers, accurate integration is not possible), 7.83 (s, 3H), 8.32 (s, 3H). ^{13}C-NMR (125 MHz, CD_2Cl_2, 25ºC,) δ (ppm) 1.3, 14.5 (C*H*$_3$), 14.9 (C*H*$_3$), 23.3, 25.7, 29.9(-C*H*$_2$*S*), 30.2(-C*H*$_2$*S*), 30.3(-C*H*$_2$*S*), 32.5, 33.7, 111.4, 120.5, 122.1, 122.4, 122.6, 124.5, 128.1, 128.5, 129.3, 130.5, 132.7, 134.3, 137.8, 138.5, 140.4, 142.0 (C*NS*), 144.0. MS (MALDI-TOF) (*m/z*): $[M]^+$ calcd. for $C_{80}H_{68}BN_7RuS_6$ 1431.3017; found 1431.3012; Elemental Analysis Calcd for $C_{80}H_{68}BN_7RuS_6$: C, 67.11; H, 4.79; N, 6.85. Found: C, 66.90; H, 4.62; N, 6.56.

ACKNOWLEDGEMENTS

This work was supported by the MEXT Program for Promoting the Enhancement of Research Universities in NAIST, the CNRS and the University Paul Sabatier (Toulouse). It has also received funding from the European Union's Horizon 2020 research and innovation program under the project MEMO, grant agreement No 766864 and from the JSPS KAKENHI grant in aid for Scientific Research on Innovative Areas "Molecular Engine (No.8006)" 18H05419. R.A. thanks the NAIST foundation for financial support. Y.G. thanks the French Ministry of National Education for a PhD Fellowship. C.J.M. thanks the JSPS KAKENHI Grant-in-Aid for Early-Career Scientists (19K15312) and G.R. the JSPS KAKENHI Grant-in-Aid for Challenging Research (20K21131). This research was also partly supported by the JSPS KAKENHI Grant Number JP26107006 in Scientific Research on Innovative Areas "Photosynergetics". The DFT calculations appearing in this article were performed using HPC resources from CALMIP (Grant 2020-p20041).

REFERENCES

(1) Balzani, V.; Credi, A.; Venturi, M. *Molecular Devices and Machines – Concepts and perspectives for the Nanoworld*, Wiley-VCH, Weinheim, 2nd ed. **2008**.

(2) Rapenne, G.; Launay, J.-P.; Joachim, C. Design and synthesis of mono-molecular machines. *J. Phys.: Condens. Matter*. **2006**, *18*, S1797–S1808.

(3) (a) Sauvage, J.-P. From chemical topology to molecular machines. *Angew. Chem. Int. Ed.* **2017**, *56*, 11080–11093. (b) Stoddart, J. F. Mechanically interlocked molecules, molecular shuttles, switches, and machines. *Angew. Chem. Int. Ed.* **2017**, *56*, 11094–11125. (c) Feringa, B. L. The Art of Building Small: From Molecular Switches to Motors. *Angew. Chem. Int. Ed.* **2017**, *56*, 11060–11078.

(4) Breslow, R. Biomimetic chemistry: biology as an inspiration. *J. Biol. Chem.* **2008**, *284*, 1337–1342.

(5) (a) Kelly, T. R.; Silva, H. D.; Silva, R. A. Unidirectional rotary motion in a molecular system. *Nature* **1999**, *401*, 150–152. (b) Koumura, N.; Zijlstra, R. W. J.; van Delden, R. A.; Harada, N.; Feringa, B. L. Light-driven monodirectional molecular rotor. *Nature* **1999**, *401*, 152–155. (c) Leigh, D. A.; Wong, J. K. Y.; Dehez, F.; Zerbetto, F. Unidirectional rotation in a mechanically interlocked molecular rotor. *Nature* **2003**, *424*, 174–179. (d) Kottas, G. S.; Clarke, L. I.; Horinek, D.; Michl, J. Artificial molecular rotors. *Chem. Rev.* **2005**, *105*, 1281–1376. (e) Kay, E. R.; Leigh, D. A.; Zerbetto, F. Synthetic molecular motors and mechanical machines. *Angew. Chem. Int. Ed.* **2007**, *46*, 72–191. (f) Perera, U. G. E.; Ample, F.; Echeverria, J.; Kersell, H.; Zhang, Y.; Vives, G.; Grisolia, M.; Rapenne, G.; Joachim, C.; Hla, S.-W. Controlled clockwise and anticlockwise rotational switching of a molecular motor. *Nature Nanotechnol.* **2013**, *8*, 46–51. (g) Zhang, Y.; Kersell, H.; Stefak, R.; Echeverria, J.; Iancu, V.; Perera, U. G. E.; Li, Y.; Deshpande, A.; Braun, K.-F.; Joachim, C.; Rapenne, G.; Hla, S.-W. Simultaneous and coordinated rotational switching of all molecular rotors in a network. *Nature Nanotechnol*. **2016**, *11*, 706–713. (h) Kassem, S.; van Leeuwen, T.; Lubbe, A. S.; Wilson, M. R.; Feringa, B. L.; Leigh, D. A. Artificial molecular motors. *Chem. Soc. Rev.* **2017**, *46*, 2592–2621. (i) García-López, V.; Liu, D.; Tour, J. M. Light-activated organic molecular motors and their applications. *Chem. Rev.* **2020**, *120*, 79–124. (j)

Goswami, A.; Saha, S.; Kumar Biswas, P.; Schmittel, M. (Nano)mechanical motion triggered by metal coordination: from functional devices to networked multicomponent catalytic machinery. *Chem. Rev.* **2020**, *120*, 125–199. (k) Baroncini, M.; Silvi, S.; Credi, A. Photo- and redox-driven artificial molecular motors. *Chem. Rev.* **2020**, *120*, 200–268.

(6) (a) Jimenez, M. C.; Dietrich-Buchecker, C.; Sauvage, J.-P. Towards synthetic molecular muscles: Contraction and stretching of a linear rotaxane dimer. *Angew. Chem. Int. Ed.* **2000**, *39*, 3284–3287. (b) Chambron, J.-C.; Dietrich-Buchecker, C.; Rapenne, G.; Sauvage, J.-P. Resolution of topologically chiral molecular objects. *Chirality* **1998**, *10*, 125–133. (c) Romuald, C.; Busseron, E.; Coutrot, F. Very contracted to extended *co*-conformations with or without oscillations in two- and three-station [c2]daisy chains. *J. Org. Chem.* **2010**, *75*, 6516–6531. (d) Du, G.; Moulin, E.; Jouault, N.; Buhler, E.; Giuseppone, N. Muscle-like supramolecular polymers: Integrated motion from thousands of molecular machines. *Angew. Chem. Int. Ed.* **2012**, *51*, 12504–12508.

(7) von Delius, M.; Geertsema, E. M.; Leigh, D. A.; Tang, D.-T. D. Design, synthesis and operation of small molecules that walk along tracks. *J. Am. Chem. Soc*. **2010**, *132*, 16134–16145.

(8) Kammerer, C.; Erbland, G.; Gisbert, Y.; Nishino, T.; Yasuhara, K.; Rapenne, G. Biomimetic and technomimetic single molecular machines. *Chem. Lett.* **2019**, *48*, 299–308.

(9) Muraoka, T.; Kinbara, K.; Kobayashi, Y.; Aida, T. Light-driven open−close motion of chiral molecular scissors. *J. Am. Chem. Soc.* **2003**, *125*, 5612–5613.

(10) (a) Hounshell, W. D.; Johnson, C. A.; Guenzi, A.; Cozzi, F.; Mislow, K. Stereochemical consequences of dynamic gearing in substituted bis(9-triptycyl) methanes and related molecules. *Proc. Natl. Acad. Sci USA* **1980**, *77*, 6961–6964. (b) Kawada, Y.; Iwamura, H. Unconventional synthesis and conformational flexibility of bis(1-triptycyl) ether. *J. Org. Chem.* **1980**, *45*, 2547–2548. (c) Frantz, D. K.; Linden, A.; Baldridge, K. K.; Siegel, J. S. Molecular Spur Gears Comprising Triptycene Rotators and Bibenzimidazole-Based Stators. *J. Am. Chem. Soc.* **2012**, *134*, 1528–1535. (d) Ube, H.; Yasuda, Y.; Sato, H.; Shionoya, M. Metal-centred azaphosphatriptycene gear with a photo- and thermally driven mechanical switching function based on coordination isomerism. *Nature Commun.* **2017**, *8*, 14296.

(11) (a) Jacquot de Rouville, H.-P.; Garbage, R.; Ample, F.; Nickel, A.; Meyer, J.; Moresco, F.; Joachim, C.; Rapenne, G. Synthesis and STM imaging of symmetric and dissymmetric ethynyl-bridged dimers of boron-subphthalocyanine bowl-shaped nano-wheels. *Chem. Eur. J.* **2012**, *18*, 8925–8928. (b) Jacquot de Rouville, H.-P.; Garbage, R.; Cook, R.E.; Pujol, A.R.; Sirven, A.M.; Rapenne, G. Synthesis of polycyclic aromatic hydrocarbon-based nanovehicles equiped with triptycene wheels. *Chem. Eur. J.* **2012**, *18*, 3023–3031. (c) Joachim, C.; Rapenne, G. Molecule concept-nanocars : chassis, wheels and motors? *ACS Nano* **2013**, *7*, 11–14.

(12) (a) Joachim, C.; Moresco, F.; Rapenne, G.; Meyer, G. The design of a nanoscale molecular barrow. *Nanotechnol*. **2002**, *13*, 330–335. (b) Rapenne, G.; Jimenez-Bueno, G. Molecular Machines : Synthesis and characterization of two prototypes of molecular wheelbarrows. *Tetrahedron* **2007**, *63*, 7018–7026.

(13) (a) Shirai, Y.; Osgood, A. J.; Zhao, Y.; Kelly, K. F.; Tour J. M. Directional Control in Thermally Driven Single-Molecule Nanocars. *Nano Lett.* **2005**, *5*, 2330–2334. (b) Vives, G.; Tour, J. M. Synthesis of Single-Molecule Nanocars. *Acc. Chem. Res.* **2009,** *42*, 473–487. (c) Kudernac, T.; Ruangsupapichat, N.; Parschau, M.; Macia, B.; Katsonis, N.; Harutyunyan, S. R.; Ernst, K.-H.; Feringa, B. L. Electrically Driven Directional Motion of a Four-Wheeled Molecule on a Metal Surface. *Nature* **2011**, *479*, 208–211. (d) Rapenne, G.; Joachim, C. World's first nanocar race: a single molecule piloted per team. *Nature Rev. Mater.* **2017**, *2*, 17040–17042.

(14) Gisbert, Y.; Abid, S.; Bertrand, G.; Saffon-Merceron, N.; Kammerer, C.; Rapenne, G. Modular synthesis of pentaarylcyclopentadienyl Ru-based molecular machines via sequential Pd-catalysed cross couplings. *Chem. Commun.* **2019**, *55*, 14689–14692.

(15) Badjić, J. D.; Credi, A.; Silvi, S.; Stoddart, J. F. A molecular elevator. *Science* **2004**, *303*, 1845–1849.

(16) Kassem, S.; Lee, A. T. L.; Leigh, D. A.; Markevicius, A.; Solá, J. Pick-up, transport and release of a molecular cargo using a small-molecule robotic arm. *Nature Chem.* **2016**, *8*, 138–143.

(17) Vives, G.; Jacquot de Rouville, H.-P.; Carella, A.; Launay, J.-P.; Rapenne, G. Prototypes of molecular motors based on star-shaped organometallic ruthenium complexes. *Chem. Soc. Rev.* **2009**, *38*, 1551–1561.

(18) Zhang, Y.; Calupitan, J. P.; Rojas, T.; Tumbleson, R.; Erbland, G.; Kammerer, C.; Ajayi, T.M.; Wang,

S.; Curtiss, L.C.; Ngo, A.T.; Ulloa, S.E.; Rapenne, G.; Hla, S.W. A chiral molecular propeller designed for unidirectional rotations on a surface. *Nature Commun.* **2019**, *10*, 3742.

(19) (a) Chantzis, A.; Cerezo, J.; Perrier, A.; Santoro, F.; Jacquemin, D. Optical Properties of Diarylethenes with TD-DFT: 0–0 Energies, Fluorescence, Stokes Shifts, and Vibronic Shapes. *J. Chem. Theory Comput.* **2014**, *10*, 3944-3957. (b) Li, X.; Zou, Q.; Ågren, H. Photochromic Diarylethenes with Heterocyclic Aromatic Rings: Correlation between Thermal Bistability and Geometrical Characters of Transition States. *J. Phys. Chem. A* **2015**, *119*, 9140-9147.

(20) (a) Irie, M. Diarylethenes for Memories and Switches. *Chem. Rev.* **2000**, *100*, 1685–1716. (b) Irie, M.; Fukaminato, T.; Matsuda, K.; Kobatake, S. Photochromism of Diarylethene Molecules and Crystals: Memories, Switches, and Actuators. *Chem. Rev.* **2014**, *114*, 12174–12277. (c) Martin, C. J.; Nakashima, T.; Rapenne, G.; Kawai, T. Recent progress in development of photoacid generators. *J. Photochem. Photobiol.* **2018**, *34*, 41–51.

(21) Carella, A.; Launay, J.-P.; Poteau, R.; Rapenne, G. Synthesis and reactivity of penta(4-halogenophenyl)cyclopentadienyl hydrotris(indazolyl)borate Ru(II) complexes : Rotation-induced Fosbury flop in an organometallic molecular turnstile. *Chem. Eur. J.* **2008**, *14*, 814–8156.

(22) Nakashima, T.; Atsumi, K.; Kawai, S.; Nakagawa, T.; Hasegawa, Y.; Kawai, T. Photochromism of Thiazole-Containing Triangle Terarylenes. *Eur. J. Org. Chem.* **2007**, *19*, 3212–3218.

(23) Kawai, S.; Nakashima, T.; Kutsunugi, Y.; Nakagawa, H.; Nakano, H.; Kawai, T. Photochromic amorphous molecular materials based on dibenzothienylthiazole structure. *J. Mater. Chem.* **2009**, *19*, 3606–3611.

(24) Yang, Y.; Weaver, M. N.; Merz, Jr., K. M. Assessment of the "6-31+G** + LANL2DZ" Mixed Basis Set Coupled with Density Functional Theory Methods and the Effective Core Potential: Prediction of Heats of Formation and Ionization Potentials for First-Row-Transition-Metal Complexes. *J. Phys. Chem. A* **2009**, *113*, 9843–9851.

(25) Uzelac, E. J.; Rasmussen, S. C. Synthesis of brominated thiazoles via sequential bromination–debromination methods. *J. Org. Chem.* **2017**, *82*, 5947−5951.

(26) Thépot, J.; Lapinte, C. A convenient synthesis of bromopentaarylcyclopentadienes containing methyl or fluorine substituents. *J. Organomet. Chem.* **2001**, *627*, 179−188.

(27) Erbland, G.; Gisbert, Y.; Rapenne, G.; Kammerer, C.; Expedient synthesis of thioether-functionalized hydrotris(indazolyl) borate as an anchoring platform for rotary molecular machines. *Eur. J. Org. Chem.* **2018**, *34*, 4731–4739.

(28) Kutsunugi, Y.; Kawai, S.; Nakashima, T.; Kawai, T. Photochromic properties of terarylene derivatives having a π-conjugation unit on central aromatic ring. *New J. Chem.* **2009**, *33*, 1368–1373.

(29) Carella, A.; Vives, G.; Cox, T.; Jaud, J.; Rapenne, G.; Launay, J.-P. Synthesis of new tripodal tri-functionalized hydrotris(indazol-1-yl)borate ligands and X-ray structure of their ruthenium cyclopentadiene complexes. *Eur. J. Inorg. Chem.* **2006**, 980–987.

(30) M. J. Frisch et al. (see Supporting Information for full author list) Gaussian 09 Revision A.02, Gaussian Inc. Wallingford CT, **2009**.